SUPPORTING INFORMATION for:

The effects of selectively blocking the electron transport layer of n-i-p perovskite solar cells with polymer particles on device performance

Amal Altujjar[a,b,*], Ran Wang[a], Xuelian Wang[a], Jennifer M. Saunders[a], Zhenyu Jia[a], Ben Spencer[a,c], Nigel Hodson[d], Janet Jacobs[c], Osama M. Alkhudhari[a], Andrew Thomas[a,c], Richard Curry[c,e] and Brian R. Saunders[a,*]

a) Department of Materials, University of Manchester, MECD, Building A, Manchester, M1 7HL, UK.

b) Basic Science Department, Deanship of Preparatory Year and Supporting Studies, Imam Abdulrahman Bin Faisal University, Dammam 34221, KSA.

c) Photon Science Institute and The Henry Royce Institute, University of Manchester, Manchester, M13 9PL, UK.

d) BioAFM Facility, Faculty of Biology, Medicine and Health, Stopford Building, University of Manchester, Oxford Road, Manchester, M13 9PT, UK.

e) Department of Electrical and Electronic Engineering, University of Manchester, Manchester M13 9PL, UK.

EXPERIMENTAL DETAILS

Materials

Styrene (Aldrich, 99%) was purified by washing with NaOH solution (1.0 M). Divinylbenzene (DVB, 80%), 2,2′-azobis(2-methylpropionamidine) dihydrochloride (AAPH, 97%), 4,4′-azobis(4-cyanovaleric acid) (ACVA, 98%), potassium persulfate (KPS, 99%)**,** DMF (99.8%), Spiro-MeOTAD (99%), 4-tertbutylpyridine (TBP, 96%), bis(trifluoromethane)sulfonimide lithium salt (Li-TFSI, 99.95%), (FK 209 Co(III) TFSI, 98%), formamidinium iodide (FAI, 99.5%), $PbBr_2$ (99.99%), CsI, (99.99%) were all purchased from Sigma Aldrich. DMSO (99.9%) and chlorobenzene (CBZ, 99.8%) was purchased from Acros. SnO_2 (15% in H_2O colloidal dispersion) was purchased from Alfa Aesar. Lead iodide (PbI_2, 99.99%) was purchased from Tokyo Chemical Industry. Methylammonium bromide (MABr, 99.5%) was purchased from Ossila. All materials were used as received. Water was deionized, distilled and of high purity.

Preparation of cationic polystyrene microgels

The polystyrene microgel (PS MG) dispersion was prepared using surfactant-free emulsion polymerization. Water (265 mL) was stirred and purged with nitrogen gas in a reactor for 60 min at 70 °C. DVB (0.086 g, 0.661 mmol) was mixed with styrene (28.6 g, 0.275 mol) and added to the reactor. The initiator solution was added after 15 min to the monomer solution. Accordingly, AAPH (0.236 g, 0.871 mmol) was dissolved in water (7.0 g) with the aid of sonication for 5 min, then added to the monomer solution. The reaction was continued for 16 h under nitrogen at 70 °C. Finally, the MG dispersion was cooled to room temperature using an ice bath. Then, a mesh filter was used to filter the dispersion. After this, the dispersion was purified five times by centrifugation and re-dispersion of the particles in water. To transfer the particles form water to CBZ, the dispersion was freeze-dried and the powder of particles were wetted by a few drops of methanol before adding the CBZ. For example, to prepare 2.0% of MG in CBZ, 20.4 mg of freeze-dried particles were wetted by

20 μL of methanol, then 900 μL of CBZ was added and the particles were dispersed using magnetic stirring at room temperature.

Preparation of anionic polystyrene microgels

Anionic PS MGs (denoted as MG-COOH) were prepared using surfactant-free emulsion polymerization. Briefly, water (265 ml) was adjusted to pH of 9.0 using NaOH solution and then added to a 500 mL reaction vessel and stirred at 200 rpm at 70 °C and deoxygenated. ACVA (0.244 g, 0.871 mmol) was dissolved in water (7.0 mL) and adjusted to pH of 11.0 using aqueous NaOH solution. DVB (0.086 g, 0.661 mmol) was mixed with styrene (28.6 g, 0.275 mol) and added to the vessel. The ACVA solution was then quickly added under a N_2 atmosphere, and the mixture stirred for 16 h. The particle dispersion (in collapsed, latex, form) was purified using repeated centrifugation and re-dispersion in water.

Film fabrication

Indium tin oxide (ITO)-coated glass substrates (20 Ω/sq-coated glass from Ossila) were etched using Zn powder and HCl (4.0 M), and cleaned by sonication in aqueous Hellmanex solution (2%), acetone, ethanol and IPA for 15 min. The substrates were dried using a nitrogen stream and then treated by UV/Ozone (UVO) for 15 min. A dilute SnO_2 solution (2.67%) was spin coated onto the substrates at 3000 rpm for 30 s and then annealed at 150 ºC for 30 min to deposit an electron transport layer. UVO was used again to reduce the surface energy. For the control system, the glass/ITO/SnO_2 substrates were used for the deposition of perovskite films. For the MG-containing devices, PS MG dispersions in CBZ were prepared using a range of particle concentrations and then spin coated dynamically at 4000 rpm for 30 s on top of the SnO_2 layer. For the UVO-MG-containing devices, UVO was applied on the spin coated MGs for 10 min prior to the deposition of the perovskite layer. The precursor solution for $Cs_{0.05}(FA_{0.85}MA_{0.15})_{0.95}Pb(I_{0.85}Br_{0.15})_3$ was prepared by dissolving CsI (0.013 g, 0.050 mmol), MABr (0.016 g, 0.143 mmol), $PbBr_2$ (0.056 g, 0.153 mmol), FAI (0.138 g, 0.802 mmol), and

PbI_2 (0.394 g, 0.855 mmol) in 0.71 mL of mixed solvent DMF/DMSO (v/v 4:1). The perovskite precursor solution was stirred at 55 °C for 2 h before use. The photoactive layer was deposited by spin coating the perovskite solution by one-step deposition using 1000 rpm for 10 s and 6000 rpm for 20 s. CBZ (200 μL) was dripped as an antisolvent in the last 10 s. The perovskite films were annealed at 110 ºC for 50 min.

UVO treatment

All UVO treatments were conducted using an Ossila UVO/Ozone cleaner. The distance from the source to the substrate surface was 10 mm. The irradiation wavelength and intensity were 185 nm and 12 $mW.cm^{-2}$, respectively. The UVO treatment time was 10 min for the UVO-PS MG coated ETL layers.

Characterization

Contact angle measurements were performed using a Kruss DSA100. Atomic force microscopy (AFM) images for the deposited MGs on glass/ITO/ SnO_2 were obtained using a Bruker Bioscope Catalyst AFM with a Nanoscope V controller (Bruker UK Ltd., Coventry, UK), operating under the Bruker Nanoscope controller software (v9.15), and mounted on a Nikon Eclipse Ti-I optical microscope (Nikon Instruments Europe B.V.). Images were captured for samples in air using ScanAsyst^{TM} (peak-force tapping) mode with ScanAsyst Air probes (Bruker S.A.S., France; nominal spring constant 0.4 N/m, radius of curvature 8nm). Image analysis was performed using the Bruker Nanoscope Analysis (v1.4) software package (Bruker Corporation, USA). Fourier-transform infrared (FTIR) spectra were measured for the freeze-dried MGs before and after UVO exposure using a Nicolet 5700 ATR-FTIR spectrometer. SEM images were captured using a Tescan Mira. UV-visible spectra were measured using an Agilent Cary 60 UV-Vis spectrophotometer. Steady-state photoluminescence (PL) spectra and time-resolved photoluminescence (TRPL) were collected using a FLS980 instrument (Edinburgh Instruments, UK). The excitation wavelength was 470 nm for PL

measurements and 405 nm for TRPL. All UV-visible, PL, and TRPL data were obtained using light incident on the glass side of the perovskite films deposited on glass/ ITO/ SnO_2 substrates unless otherwise stated. XRD patterns were measured using an XRD5-PANaytical X'Pert Pro X-ray diffractometer. X-ray photoelectron spectroscopy (XPS) was conducted using Al Kα X-rays (15 kV, 300 W at 20 mA emission) and an Argus electron energy analyser (ESCA2SR, Scienta Omicron GmbH). Survey spectra were measured with pass energy 150 eV and high resolution spectra using 50 eV pass energy. Binding energy calibration was performed using the C-C component of C 1s (the lowest binding energy component here) calibrated to 284.8 eV.

Device fabrication

The films were prepared as described above. Then a Spiro-OMeTAD solution (90 mg in 1.0 mL of CBZ) was mixed with TBP (34 μL), Li-TFSI (19 μL) and FK 209 Co (III) TFSI (10 μL) and spin-coated onto the glass/ITO/SnO_2/MG/perovskite at 3000 rpm for 30 s. The preparation and deposition of perovskite and Spiro layers were performed inside a glovebox with a humidity of 5.0%. The films were then kept in an oxidation chamber overnight to oxidize the Spiro. Finally, the Au contact electrode (80 nm) was deposited on top of the Spiro using a thermal evaporator.

Device characterization

Electrochemical impedance spectroscopy (EIS) data were measured under illumination (0.35 suns) using phase-sensitive detection of the current through the device. The measurements were made at the open circuit voltage with a superimposed AC voltage (20 mV) supplied using an Agilent 33210 A function generator. The device area used was 0.025 cm^2 for the EIS measurements. SCLC measurements were obtained using electron-only devices where $PC_{61}BM$ replaced the Spiro layer. Current-voltage (*J-V*) measurements were performed in ambient air using an ABET solar simulator with AM 1.5G irradiation and a Keithley 2420 Sourcemeter. The active area of the devices as defined by a mask was 0.079 cm^2. Unless otherwise stated, the PCEs and other data discussed in this work

are from the reverse scans. A Newport QuantX-300 instrument was used to obtain EQE measurements.

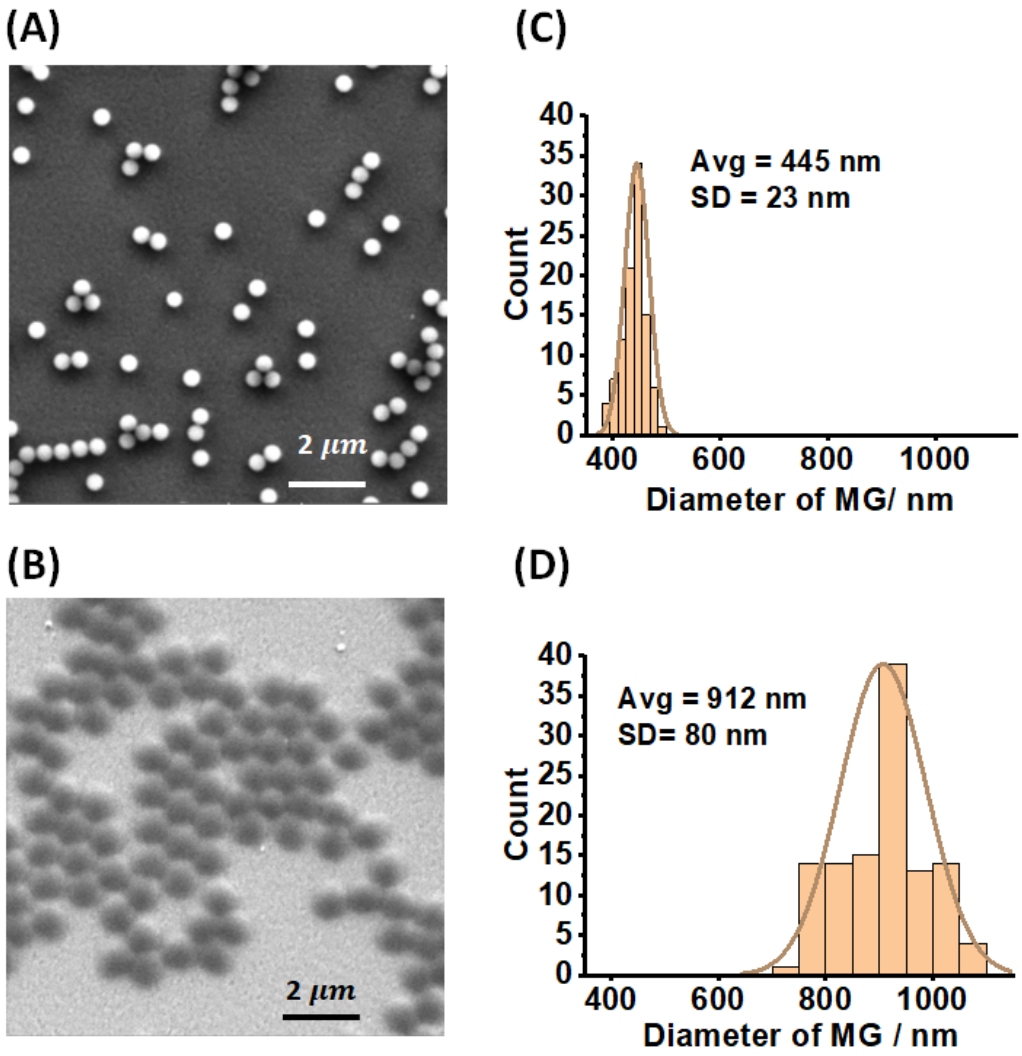

Figure S1. (A) and **(B)** SEM images for MGs deposited from water and CBZ, respectively. **(C)** and **(D)** Size distributions for the particles shown in (A) and (B), respectively.

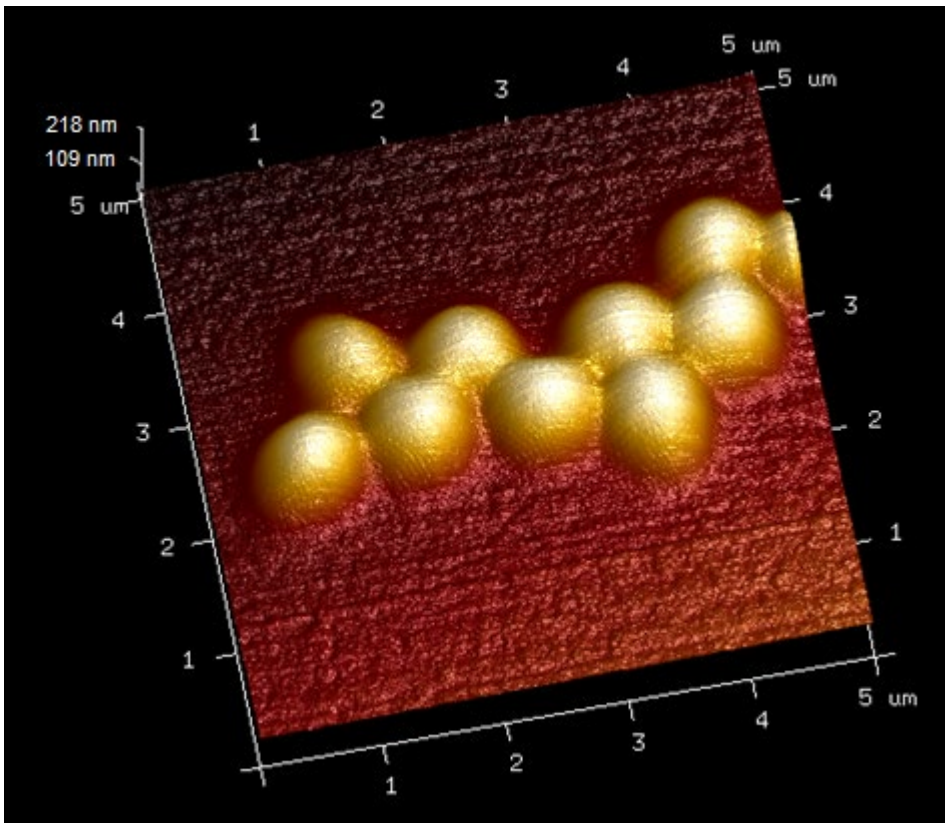

Figure S2. A 3D AFM image of inter-meshing MG particles.

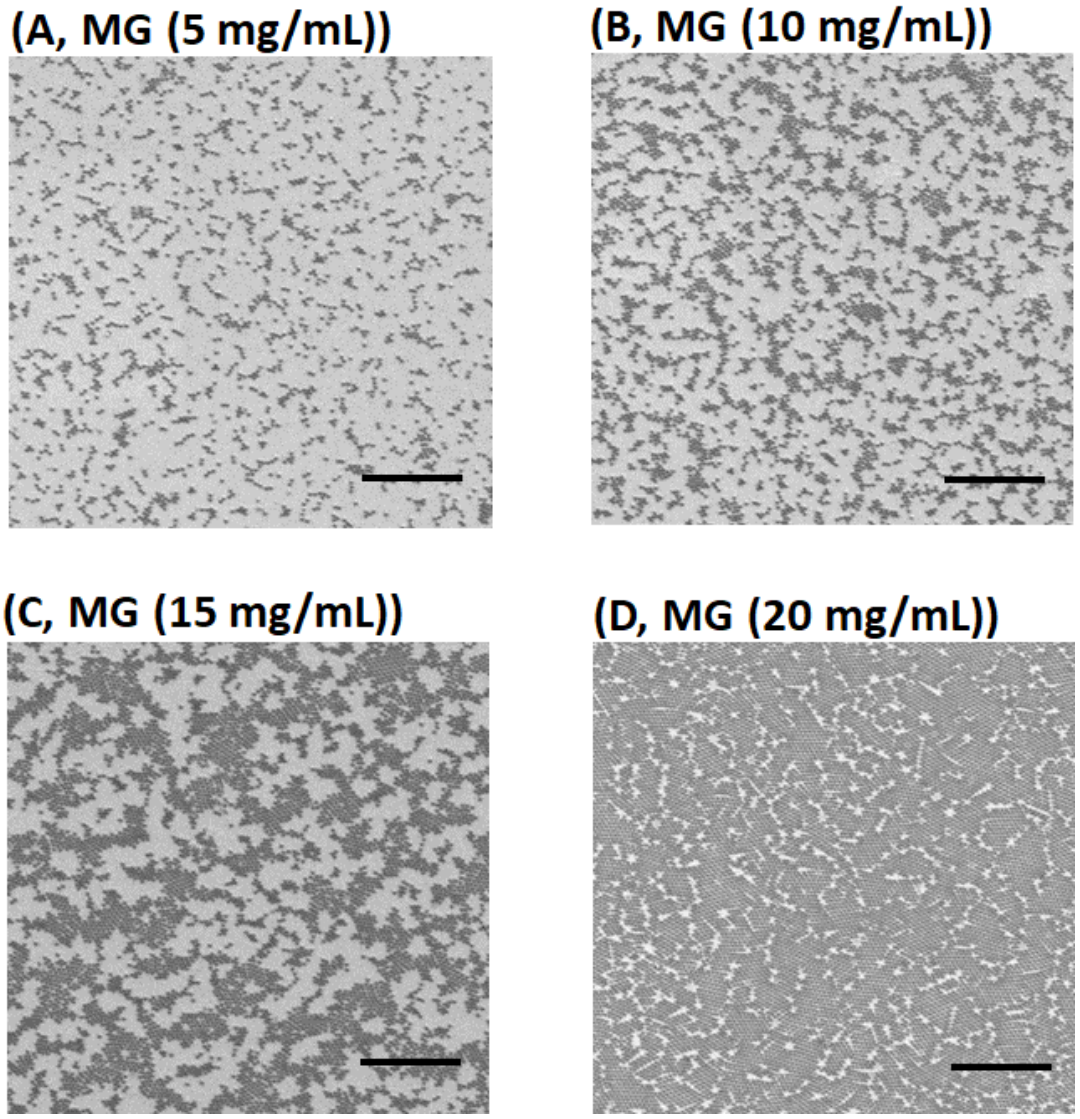

Figure S3. (A) – (D) SEM images of glass/ITO/SnO_2 substrates covered with MGs deposited using different concentrations (shown) in CBZ. The scale bars are 20 μm.

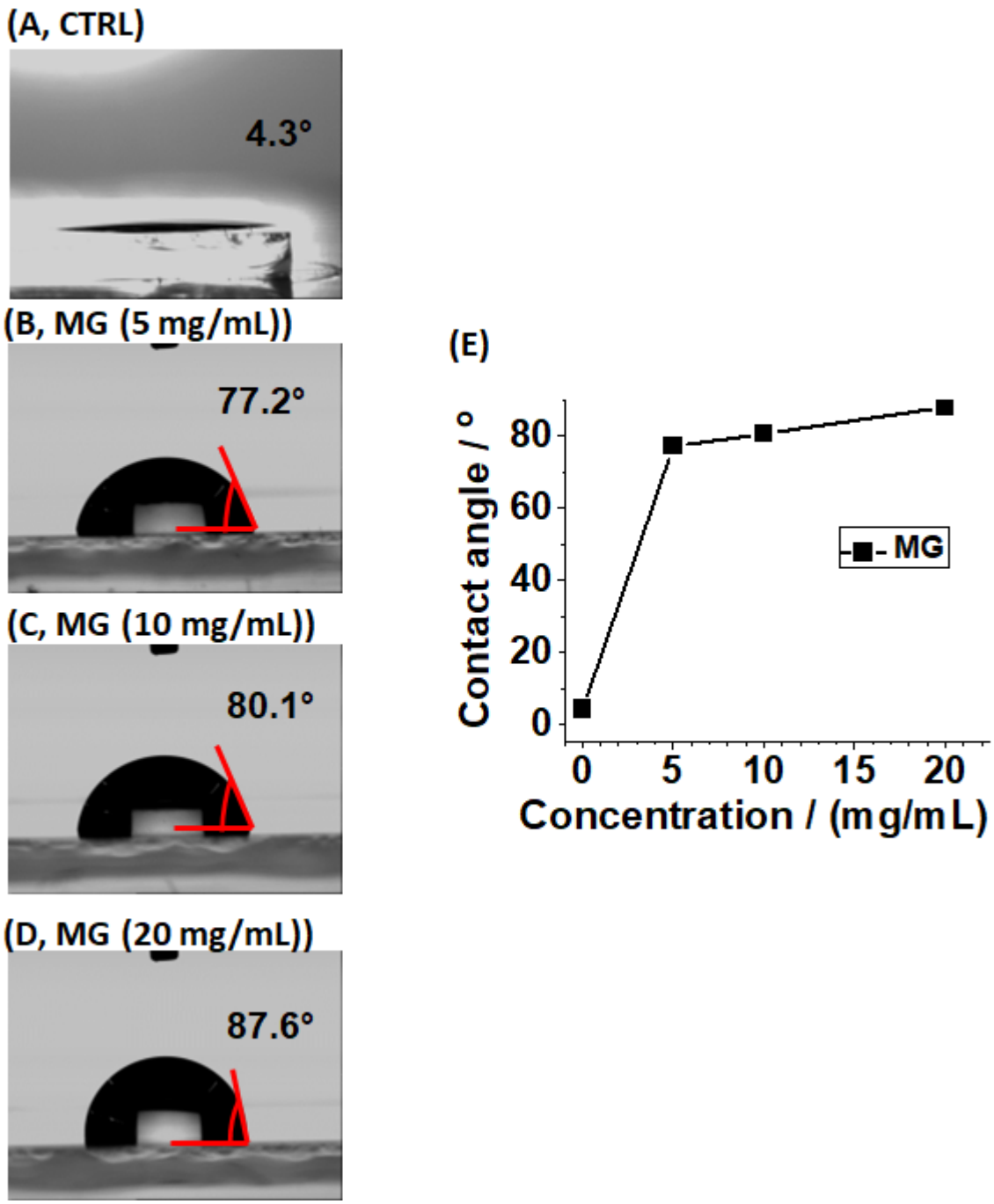

Figure S4. (A) – (D) Contact angle data for water droplets on glass/ITO/SnO_2 substrates coated with MG particles deposited at a range of concentrations (shown). **(E)** Plot of the contact angles vs. MG concentration used.

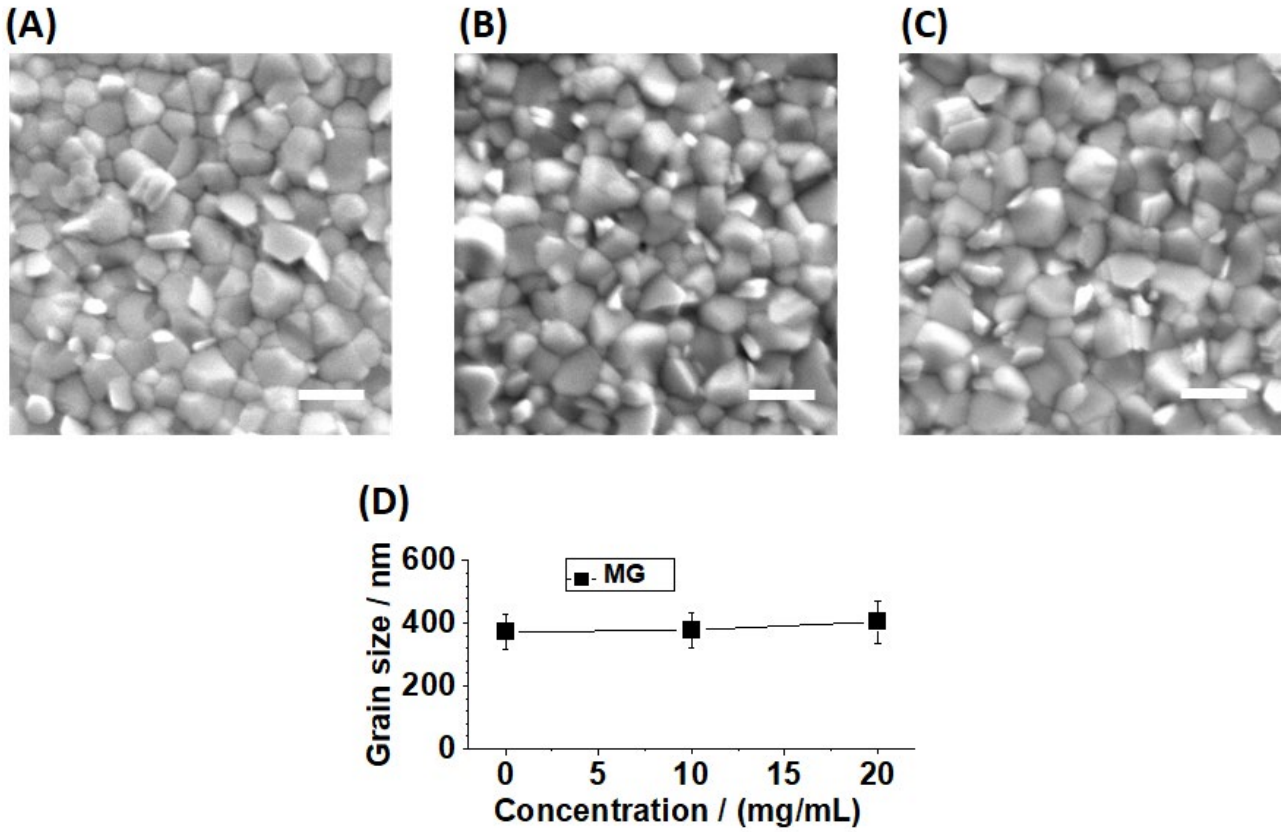

Figure S5. Top view SEM images for perovskite films deposited on top of glass/ITO/SnO_2/MG substrates prepared using MG concentrations of **(A)** 0, **(B)** 10 and **(C)** 20 mg/mL. The scale bars are 500 nm. **(D)** Average grain size as a function of MG concentration.

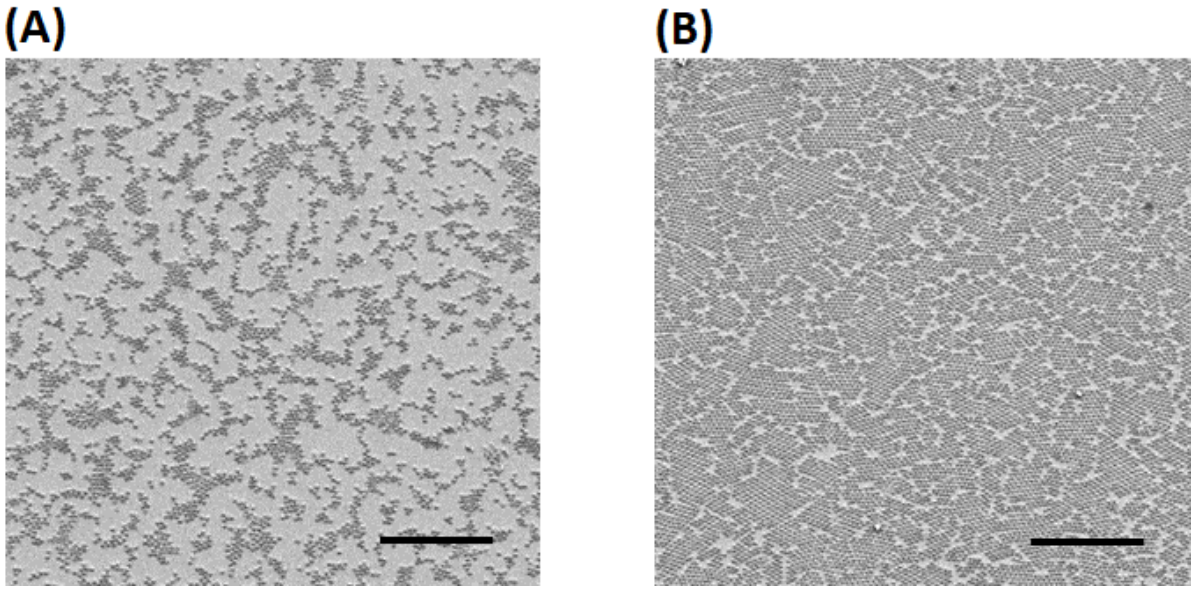

Figure S6. (A) and **(B)** SEM images of the MG particles deposited at 10 mg/mL and 20 mg/mL, respectively, after washing the perovskite layer deposited on top of these particles by water. Water dissolves the perovskite but does not swell or desorb the PS MGs. The scale bars are 20 μm.

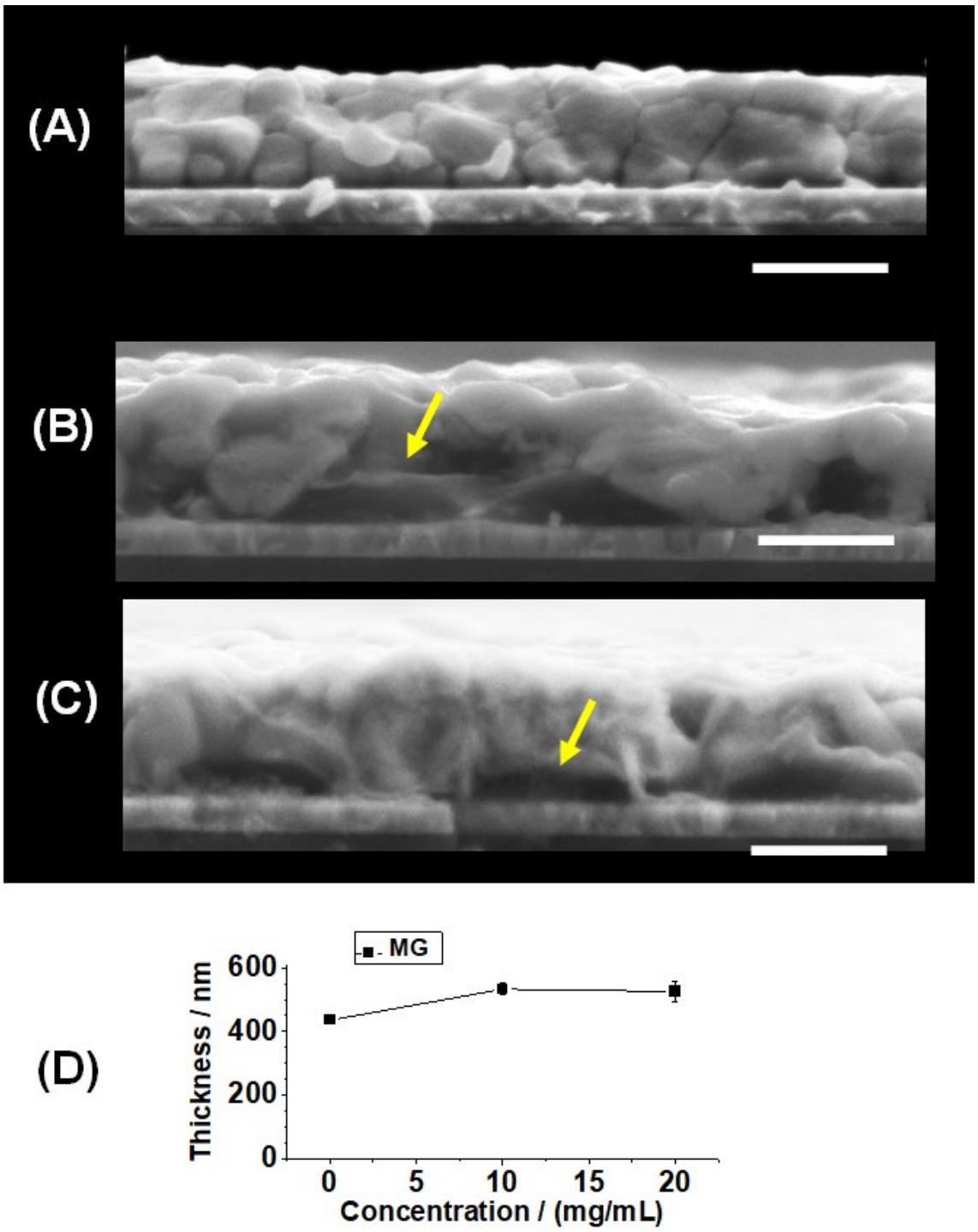

Figure S7. Cross-section SEM images for perovskite films deposited on glass/ITO/SnO_2 substrates that contained MGs deposited at concentrations of **(A)** 0, **(B)** 10 and **(C)** 20 mg/mL. The scale bars are 500 nm. The arrows highlight MG locations. The MGs appear black against the highly electron-rich perovskite phase. **(D)** Average thickness of perovskite films as a function of MG concentration.

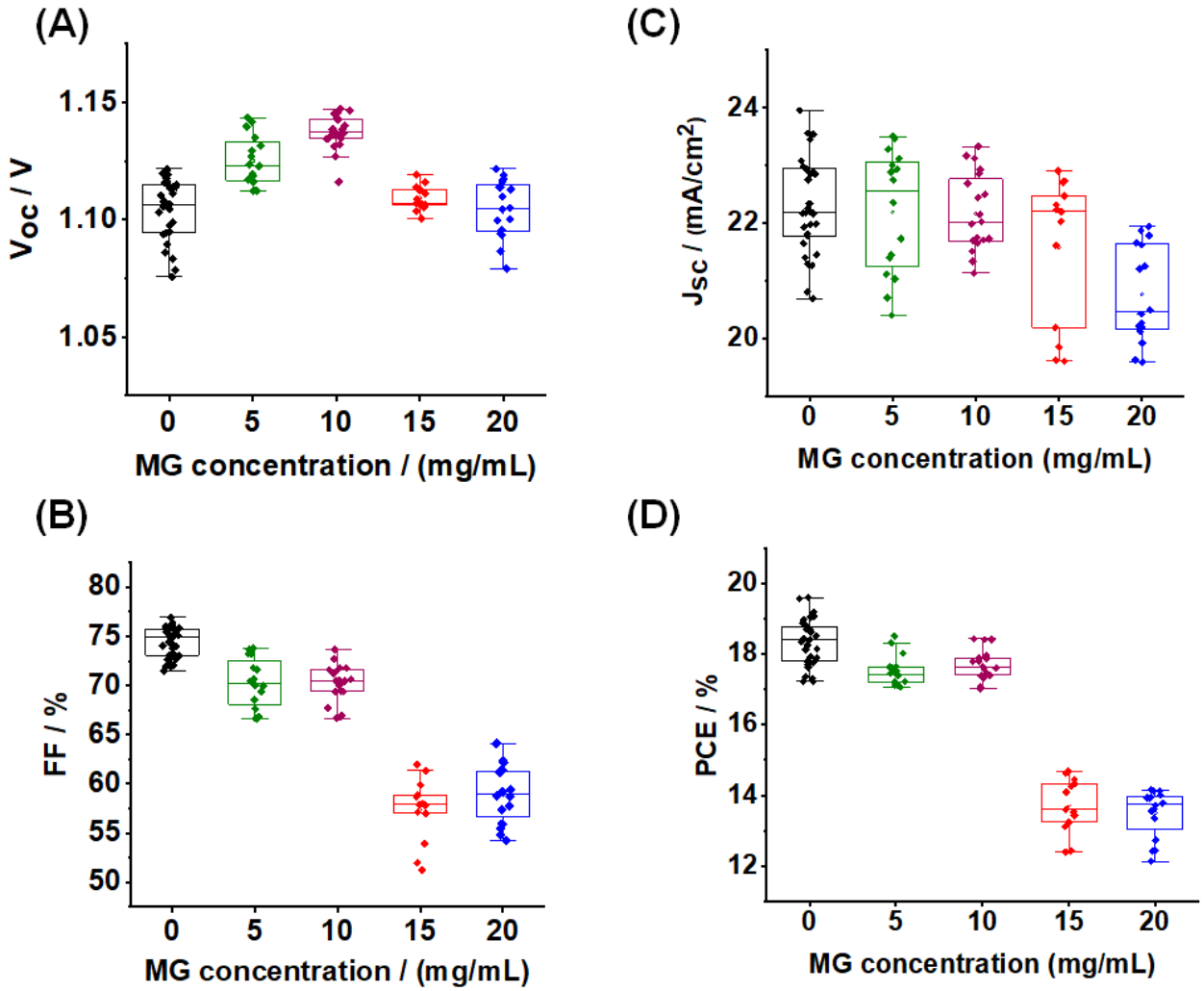

Figure S8. Box plots of performance parameters for the devices.

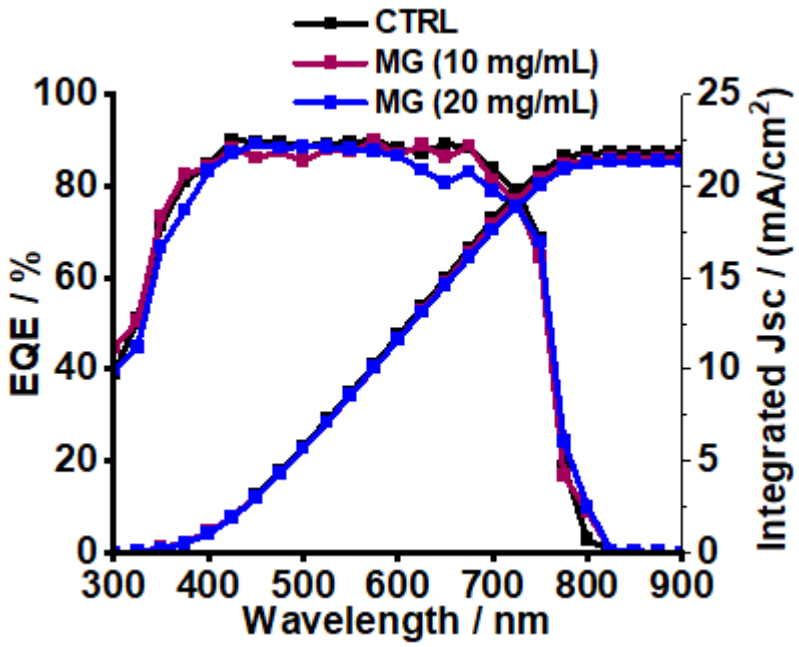

Figure S9. EQE spectra measured for various devices.

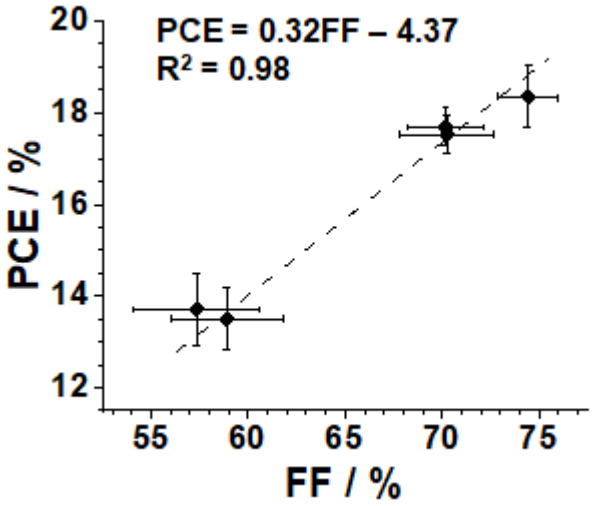

Figure S10. Variation of PCE with FF for the devices.

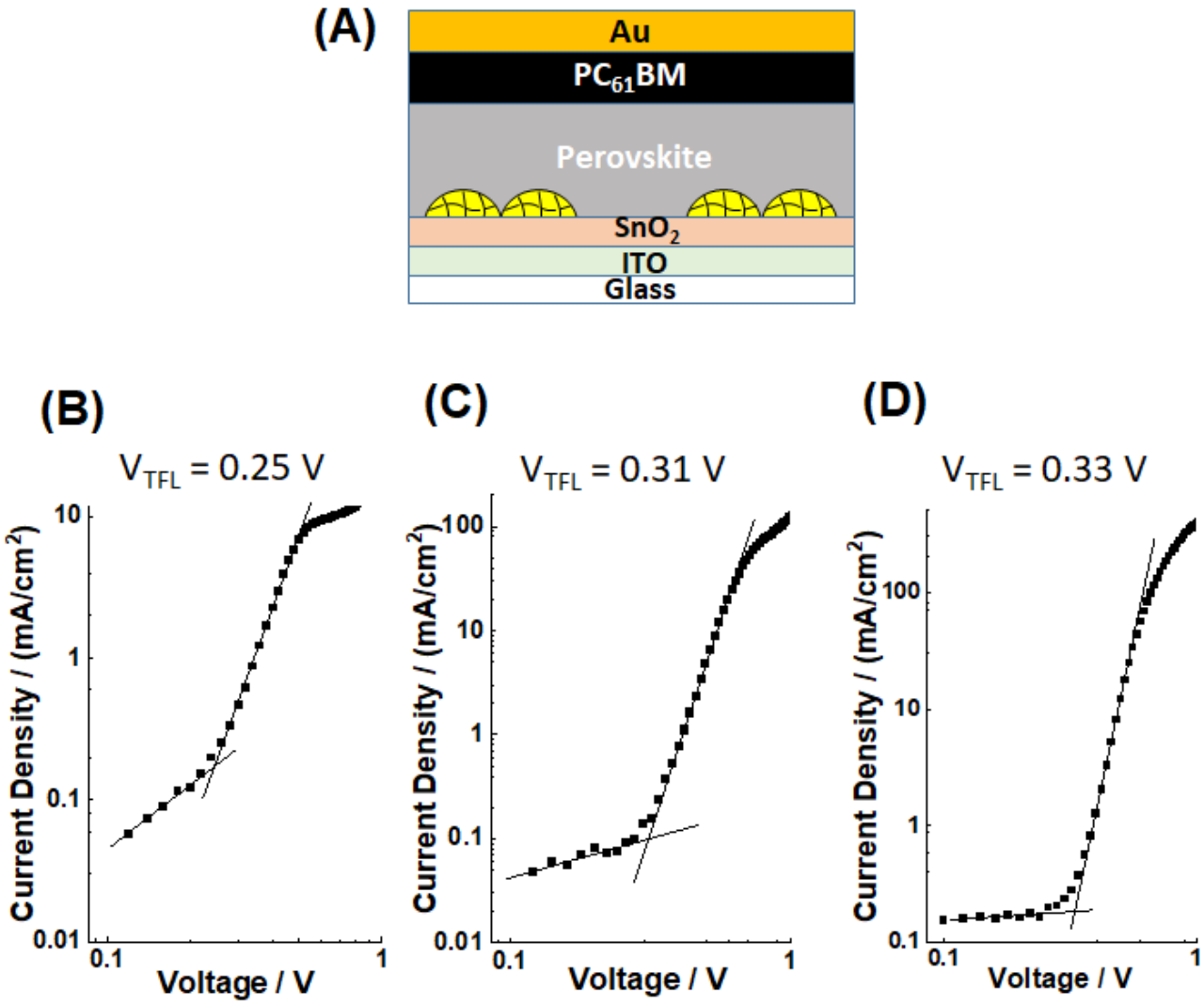

Figure S11. (A) Device geometry for SCLC measurements. *J-V* curves and the trap-filled voltage values for the **(B)** CTRL, **(C)** 10 mg/mL and **(D)** 20 mg/mL systems.

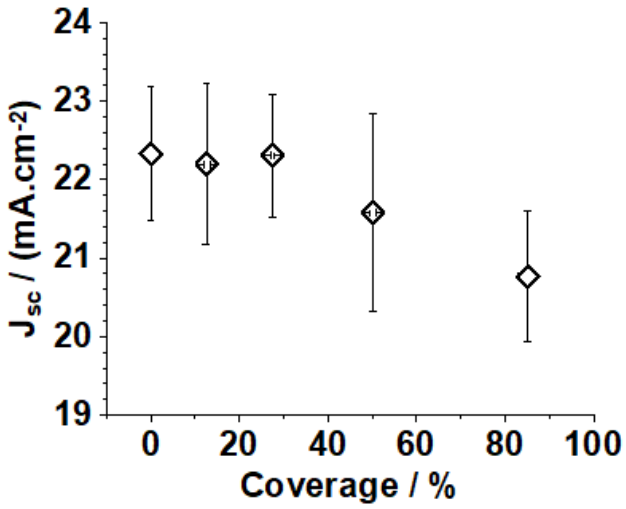

Figure S12. Variation of the short-circuit current density with coverage of the ETL by the MGs. These data were obtained from Fig. 2C.

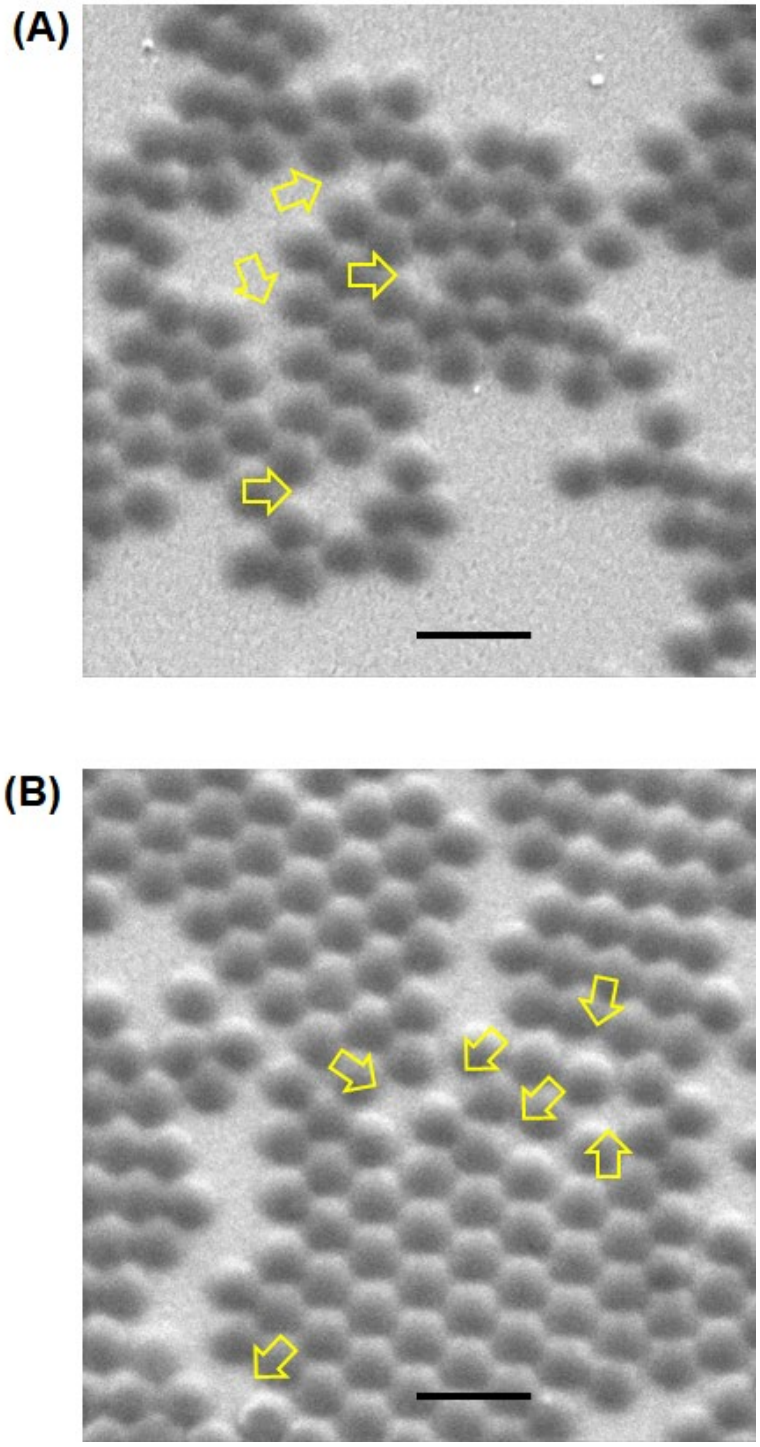

Figure S13. Expanded view SEM images showing packing errors that leave gaps within MG close packed islands for MGs spin-coated at **(A)** 15 mg/mL and **(B)** 20 mg/mL. The scale bars are 2 μm.

Additional Note S1: Using anionic polystyrene microgels to study buried interface passivation

We investigated the effect of PS MG charge on the passivation by synthesizing *anionic* PS MGs that were carboxylate functionalized. This system is denoted as MG-COOH. The zeta potential of the particles dispersed in water was -28.1 ± 0.5 mV at pH 6.7, confirming the MG-COOH particles are negatively charged in water (due to $-COO^-$ groups). MG-COOH particles that had been dispersed in CBZ (a good solvent for PS) and deposited onto glass/ITO/SnO_2 were examined using AFM (Fig. S14A). The deposited particles had a diameter and height of 1200 nm and 150 nm, respectively, with an aspect ratio of 8.0, which shows that the particles flattened considerably. The spin-coated MG-COOH particles formed micro-sized islands on glass/ITO/SnO_2 (Fig. S14B) as determined from SEM. The coverage of the ETL was measured as 24.9% when the MG-COOH concentration used was 10 mg/mL.

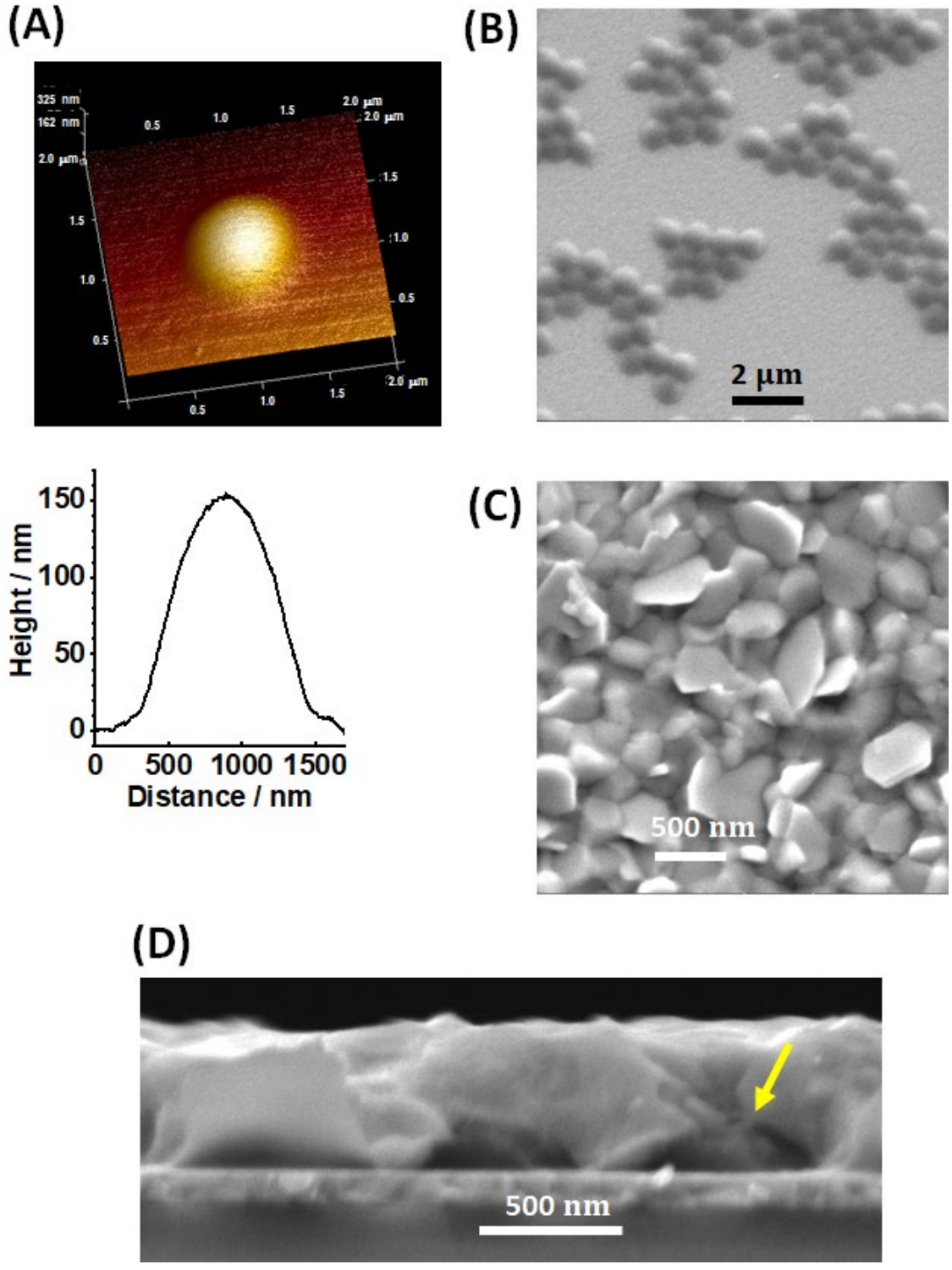

Figure S14. **(A)** A 3D AFM perspective image and a line profile for a representative MG-COOH particle. **(B)** SEM image of MG-COOH particles deposited on glass/ITO/SnO_2 using a concentration of 10 mg/mL. **(C)** Top view and **(D)** cross-sectional SEM images for perovskite films deposited on top of glass/ITO/SnO_2/MG-COOH substrates prepared using a MG-COOH concentration of 10 mg/mL. A buried MG-COOH particle is highlighted with an arrow in (D).

Perovskite films formed on the glass/ITO/SnO_2/MG-COOH substrate had an average grain size of 373 ± 8 nm (Fig. S14C). Buried MG-COOH particles are evident at the ETL/perovskite interface from the SEM cross-sectional image (Fig. S14D). The average perovskite film thickness is 531 ± 20 nm. These data show that the morphologies of the perovskite films and the buried MG-COOH particles are similar with those observed for the films prepared using the cationic MGs containing amine functional groups (see Fig. S5 and S7).

We constructed PSCs that contained buried MG-COOH particles deposited at a concentration of 10 mg/mL to assess whether an increase in V_{oc} would occur for these MGs. Box plots for the device parameters are shown in Fig. S15 and the data appear in Table S1. The highest PCE value is 17.73%. This value is relatively low compared to the control due to decreased J_{sc} and FF values. Importantly, the V_{oc} values *increased* compared to the control values (Fig. S15A). This is the same trend as evidence for the devices that were prepared using the amine-functionalized MGs (Fig. 2C). Consequently, we conclude that the nature of the charge on the MG particles is *not* responsible for the V_{oc} increases observed in Fig. 2C and Fig. S15A.

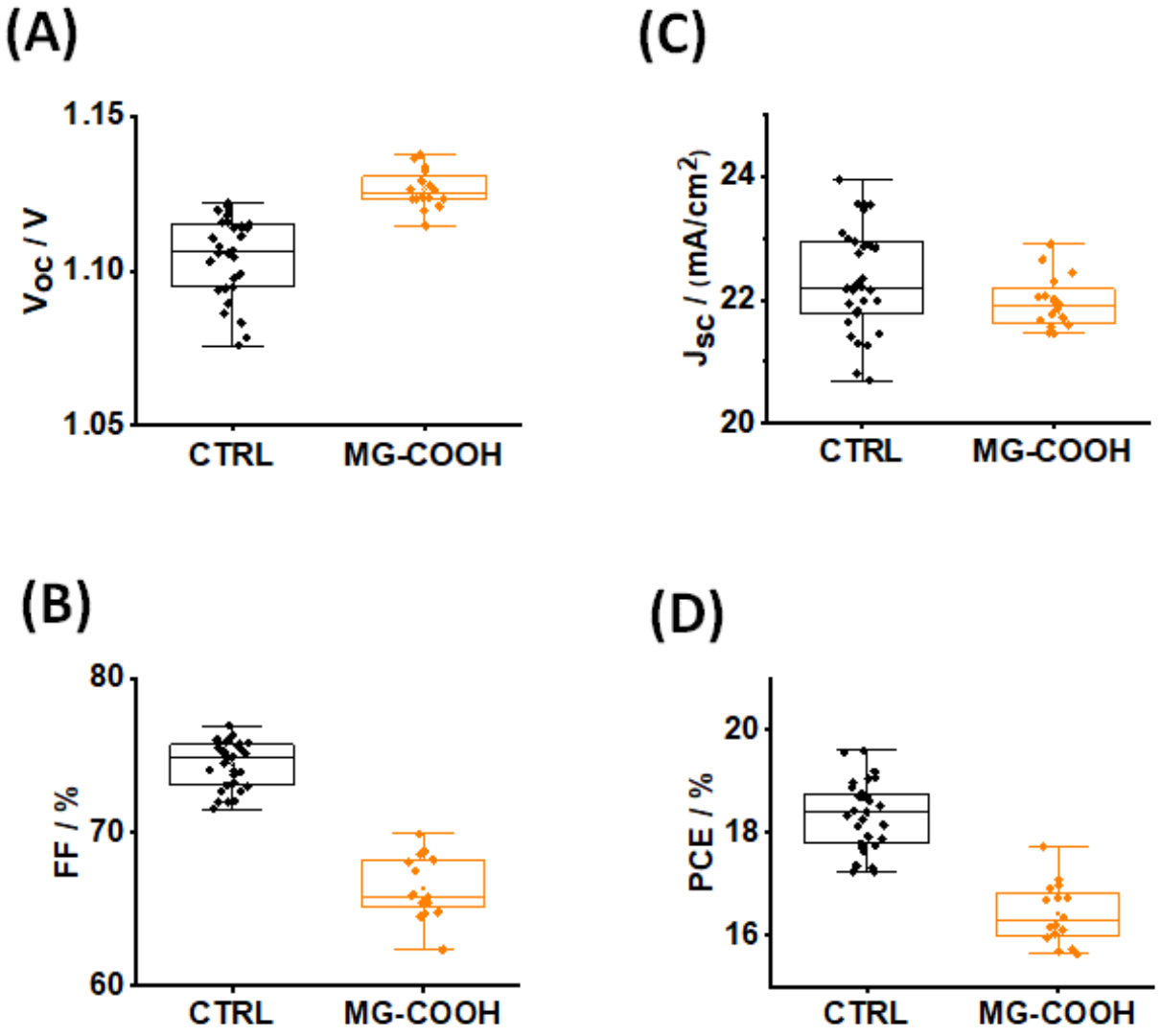

Figure S15. PSC performance parameters (**(A)** – **(D)**) for devices prepared using 10 mg/mL MG-COOH. Data for the control are shown for comparison.

We investigated passivation by measuring steady-state PL spectra of glass/ITO/SnO_2/MG-COOH/perovskite films using irradiation from the glass side (Fig. S16A)). The PL intensity is higher for the film prepared using MG-COOH compared to the control. We conducted time-resolved PL measurements (Fig. S16B). The decay is considerably slower for the perovskite film that had MG-COOH layer and the decay time was 199.4 ns (Table S2). This trend supports the steady state PL data and shows that there is less non-radiative recombination for the ETLs partially covered with MG-COOH particles than the control. Coupled with the V_{oc} data for the devices (Fig. S15A), these data show strong evidence for passivation within the films and devices prepared using the MG-COOH particles. These data reveal that the passivation caused by the MGs is not sensitive to the nature of the charge on the PS MGs, but it is attributed to a partial blocking effect whereby SnO_2 recombination centres are prevented from trapping photogenerated charges.

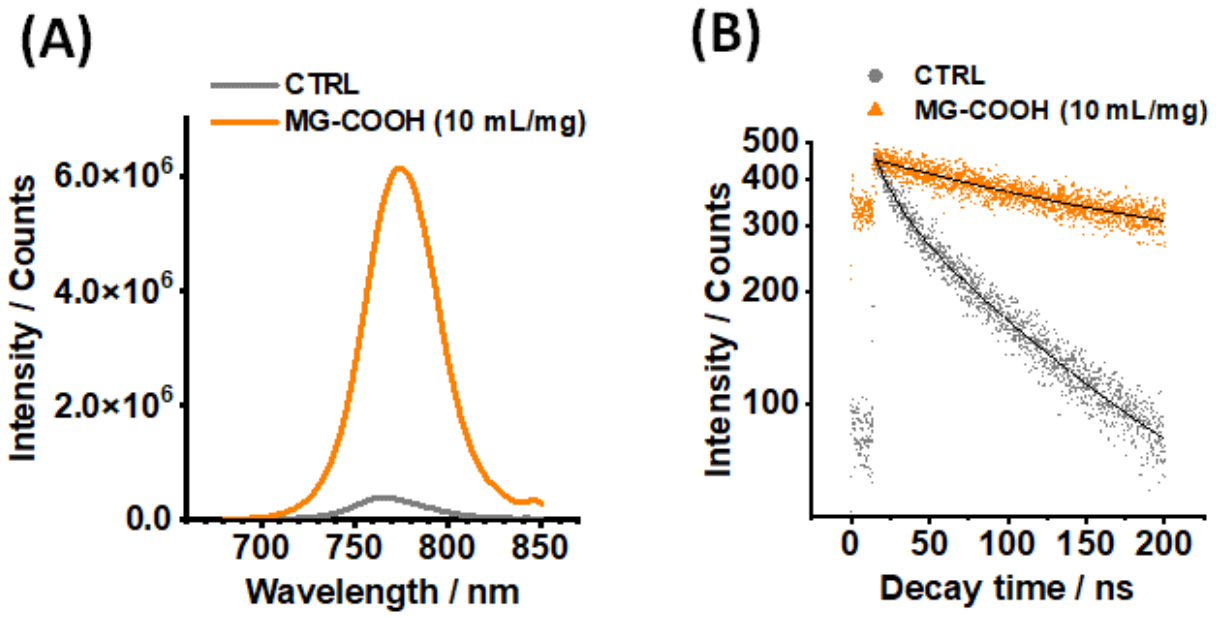

Figure S16. **(A)** Steady-state PL spectra and **(B)** TRPL data for perovskite films deposited on glass/ITO/SnO_2 substrates partially coated with MG-COOH particles. The MG-COOH concentration used was 10 mg/mL. Data for the control film is shown for comparison.

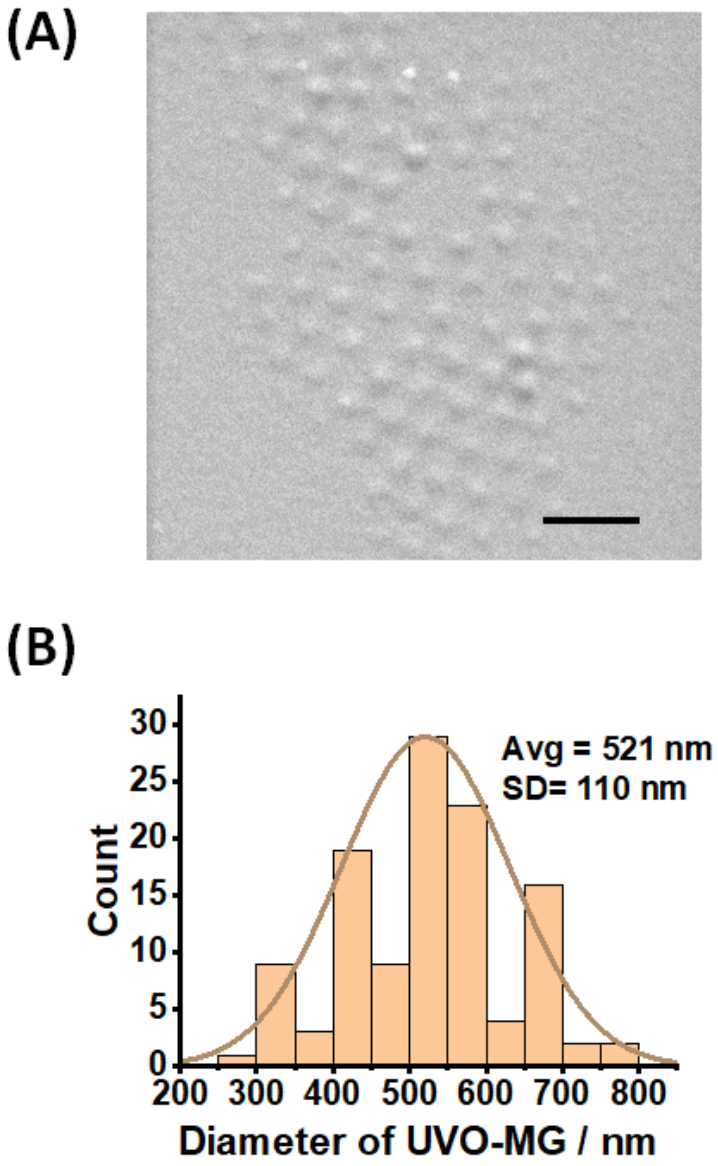

Figure S17. (A) A SEM image of MGs deposited at 10 mg/mL and then subjected to UVO treatment before the deposition of the perovskite layer. The perovskite layer was then deposited and subsequently washed away with water before imaging. The scale bar is 2 μm. **(B)** Size distribution for the UVO-MG particles shown in (A).

Additional Note S2: Chemical changes to PS MGs as a result of UV/Ozone treatment

UV/Ozone (UVO) treatment is a well-known surface treatment that etches surfaces and introduces oxygen groups. A number of studies have reported the treatment of conventional PS with UVO[1, 2]. In the present study, the UVO altered the composition of the PS MGs. FTIR spectra (Fig. S18) and XPS spectra (Fig. S19) show that the UVO treatment introduced C=O, –C-O and –N-C=O groups in the PS MGs[1-3].

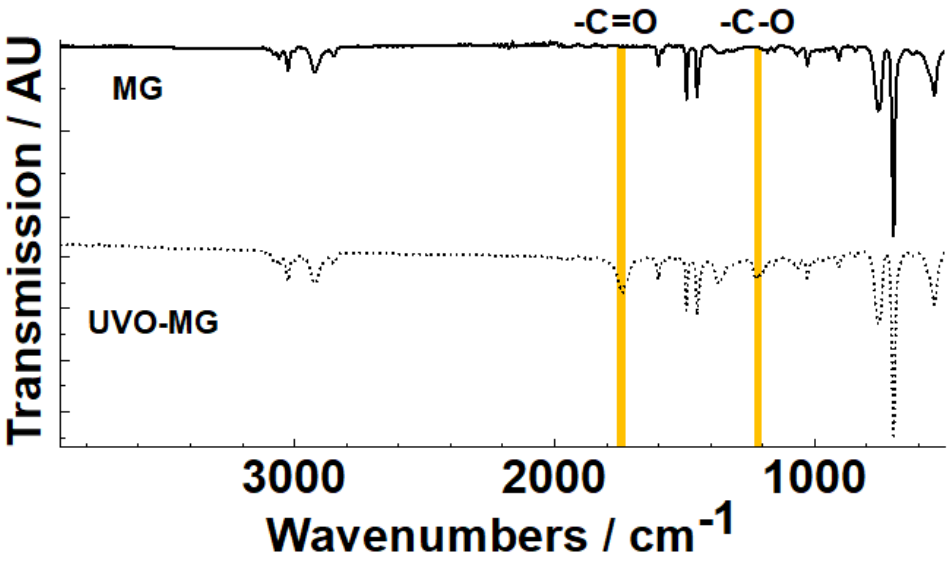

Figure S18. FTIR spectra for MGs before and after UVO treatment.

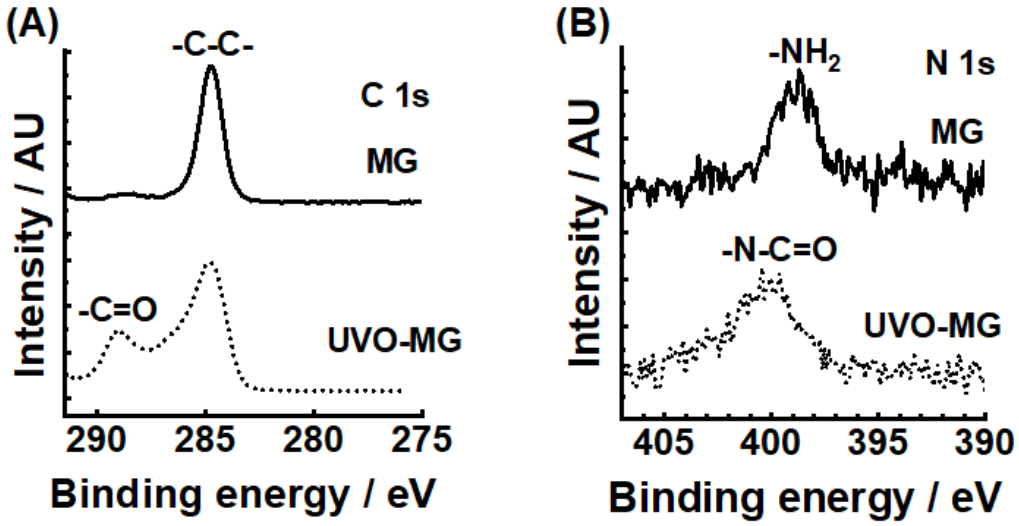

Figure S19. (A) and **(B)** XPS C 1s and N 1s core level spectra, respectively, for MGs deposited on glass/ITO/SnO_2 before and after UVO treatment.

Data from zeta potential measurements of the dispersed particles (Fig. S20) show they retain their positive charge due to the amine groups from the initiator used for MG synthesis. Furthermore, the fact that the zeta potentials are positive shows that these amine groups are present at the periphery of the MG particles. The data also show that the amine groups are not removed by the UVO treatment.

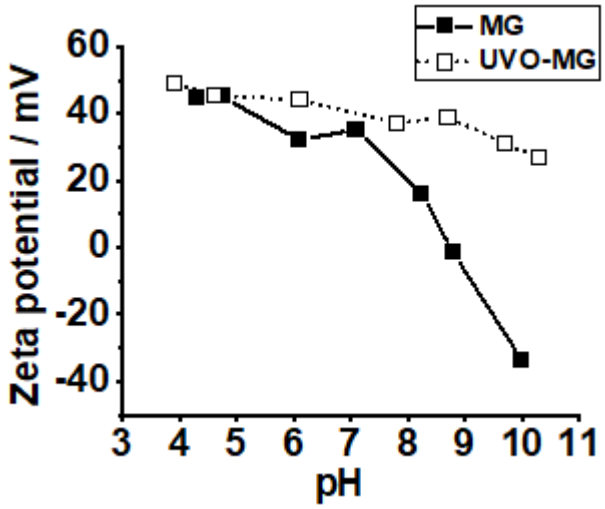

Figure S20. Zeta potential measurements for PS MGs and UVO-MGs dispersed in water.

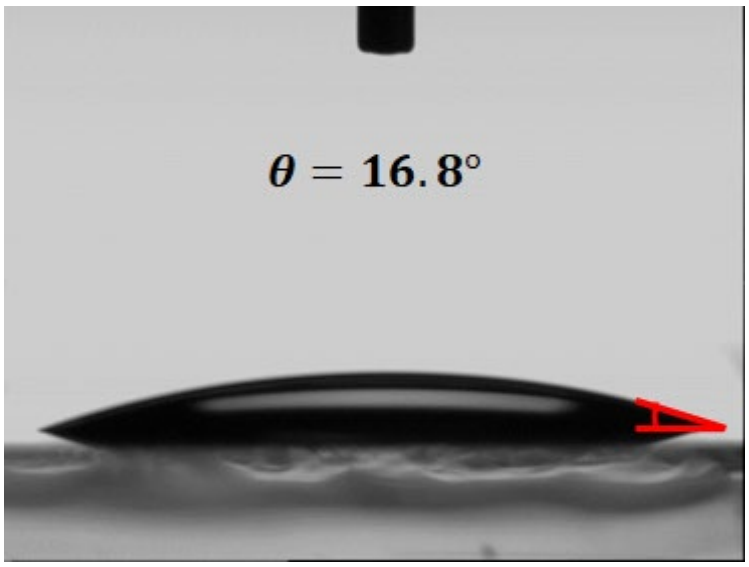

Figure S21. Contact angle measurement for water droplet on a glass/ITO/SnO_2 substrate coated with MG particles deposited at 10 mg/mL and subjected to UVO treatment.

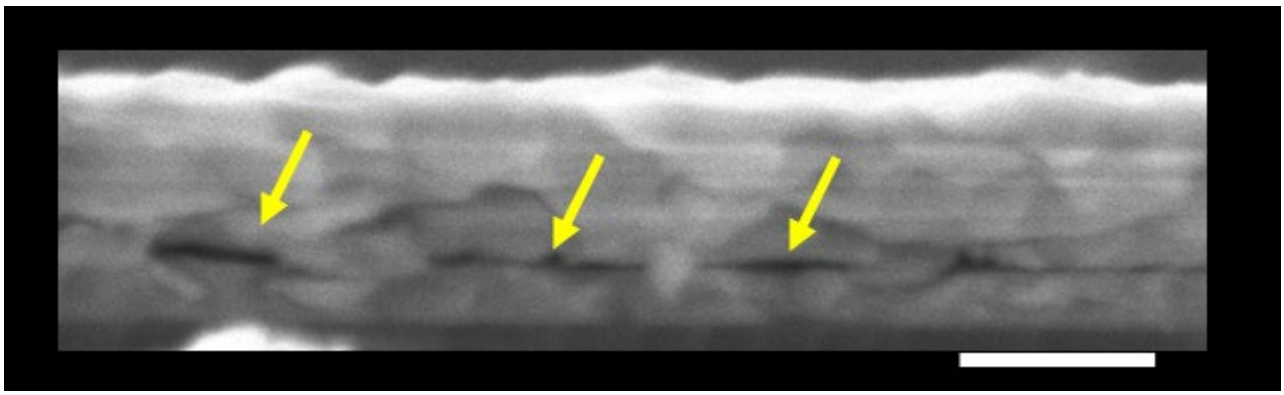

Figure S22. A cross-sectional SEM image of a perovskite film deposited on a glass/ITO/SnO_2 substrate that contained UVO-MGs deposited with a concentration of 10 mg/mL. The scale bar is 500 nm. The arrows highlight UVO- MGs.

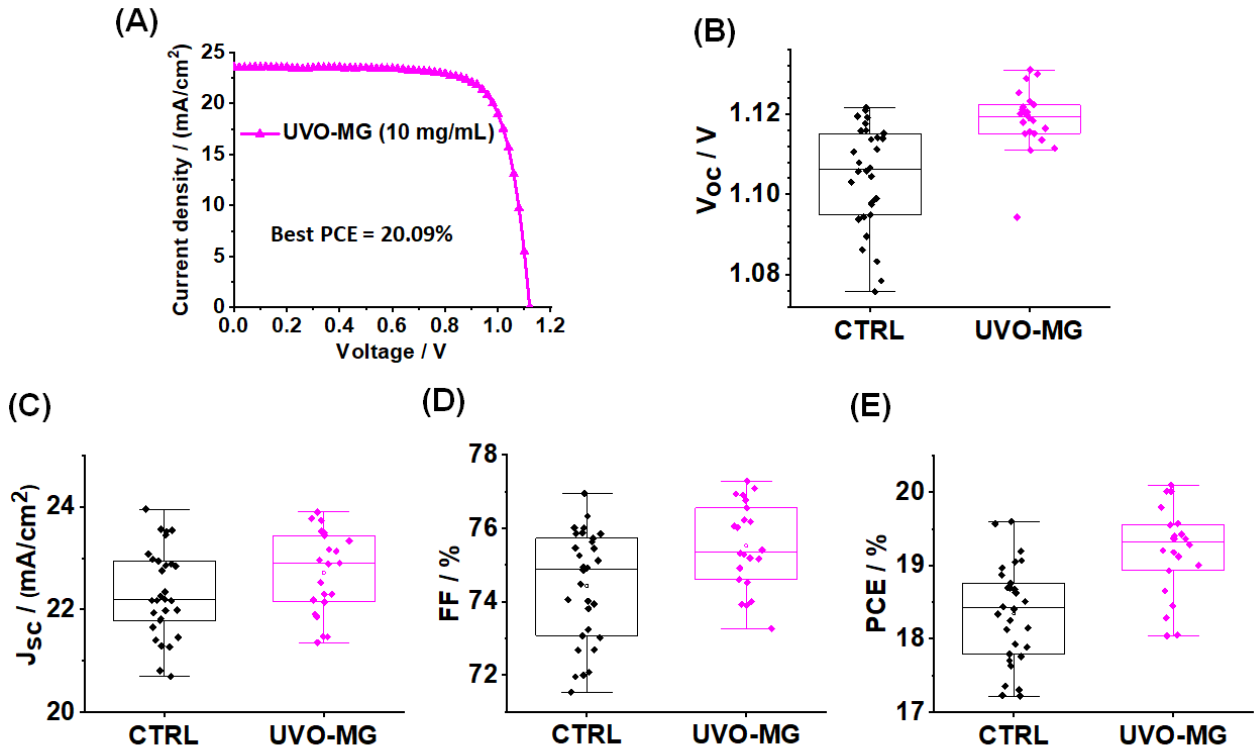

Figure S23. (A) A *J-V* curve for the best device in this study. **(B)** – **(E)** Box plots showing the performance parameters for the 10 mg/mL UVO-MG devices compared to the control.

Additional Note S3: Applying the Students t-test to the PCE data for key systems studied

We used the Student's t-test to assess whether the PCE measured for the UVO-MG-based devices and the control (Fig. 4C) are significantly different. The *null* hypothesis assumes that there is no difference between the PCE data measured for the UVO-MG-based and control devices with an exacting threshold probability of 0.001. To estimate the correctness of the null hypothesis, we employed the independent two-sample t-test to compare the PCE values for both systems using[4]:

$$t = \frac{\overline{x_1} - \overline{x_2}}{\sqrt{\left(\frac{s_1^2}{n_1} + \frac{s_2^2}{n_2}\right)}} \qquad \text{(S1)}$$

where x_1 and x_2 are the mean values of samples 1 and 2, respectively. The values of s_1 and s_2 are the respective standard deviations, and n_1 and n_2 are the number of observations for each sample. The t values were calculated for each system and then used to obtain the probability (P) values[5]. The later values are compared with the threshold value (0.001). The results (Table S4) showed that the calculated P values are much less than 0.001, which means the null hypothesis is not correct. Hence, *the average PCE for the UVO-MG system is significantly higher than that for the control*.

Additionally, the same test was applied for the MG and UVO-MG systems and the *null* hypothesis assumes that there is no difference between the PCE data measured for UVO-MG- and MG-based devices with a threshold probability of 0.001. The results (Table S4) indicate that the null hypothesis failed for these two systems. Hence, *the average PCE for the UVO-MG system is significantly higher than that for the MG-based system*.

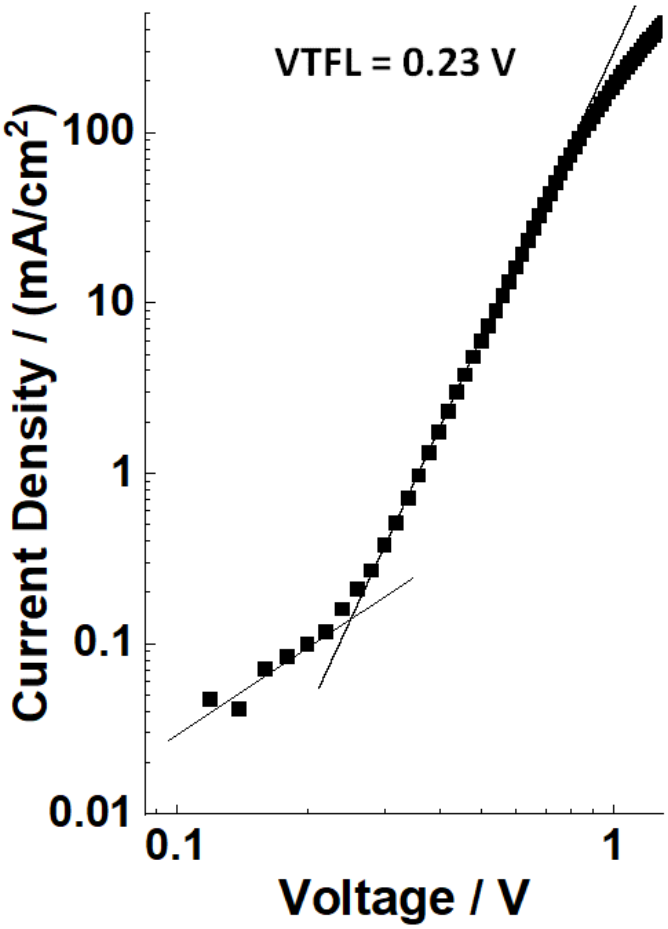

Figure S24. SCLC data for an electron-only device (geometry shown in Fig. S11A) prepared using UVO-MG (10 mg/mL).

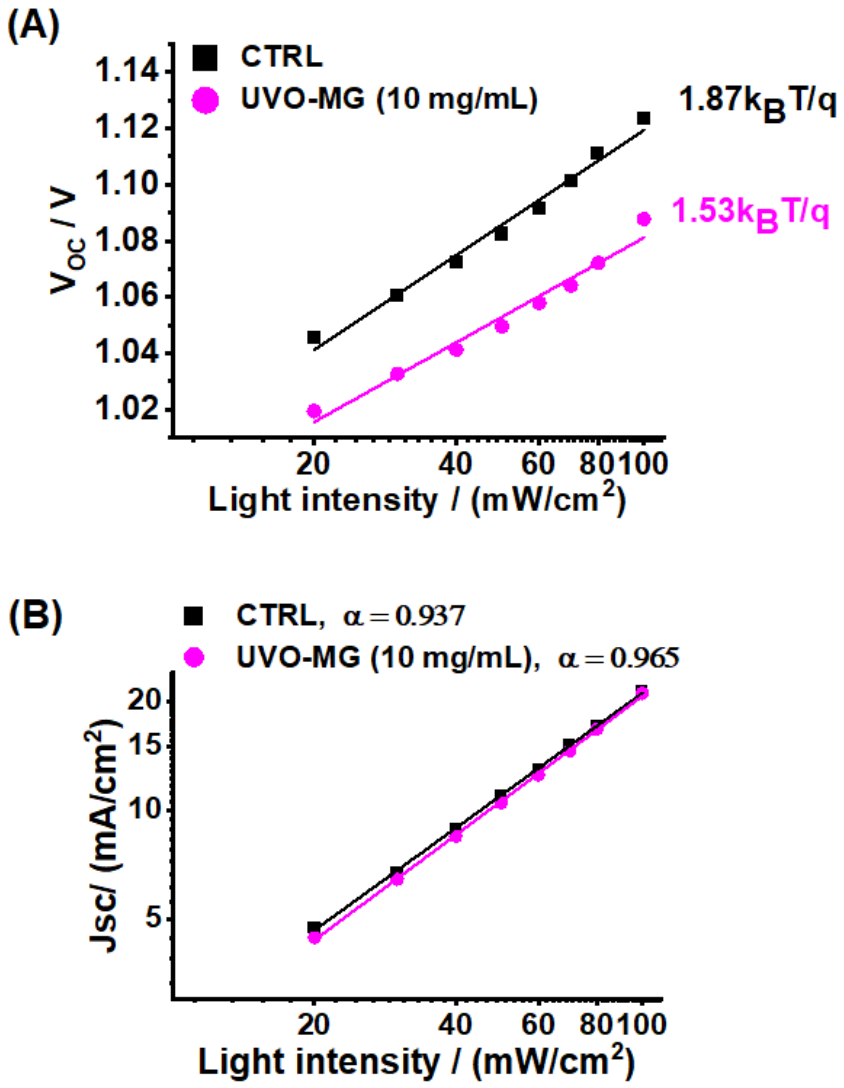

Figure S25. Variation of **(A)** open-circuit voltage and **(B)** short-circuit current density with light intensity for the control system and device prepared using UVO-MG (10 mg/mL).

Table S1. Measured photovoltaic parameters for the PSCs studied.

Particles Concentration (%)	**Scan direction**	V_{oc} **(volts)**	J_{sc} **(mA.cm^{-2})**	**FF (%)**	**PCE (%)**	**HI (%)[a]**
Control	Fwd	1.089 ± 0.016	22.33 ± 0.84	65.89 ± 1.73	16.04 ± 0.91	12.58
	Rev	1.104 ± 0.013	22.33 ± 0.85	74.43 ± 1.52	18.35 ± 0.67	
	Best	**1.119**	**22.76**	**76.95**	**19.60**	
MG (5 mg/mL)	Fwd	1.117 ± 0.010	22.25 ± 1.03	65.54 ± 1.72	16.28 ± 0.61	7.11
	Rev	1.125 ± 0.010	22.20 ± 1.02	70.26 ± 2.44	17.53 ± 0.42	
	Best	**1.127**	**22.88**	**71.80**	**18.52**	
MG (10 mg/mL)	Fwd	1.132 ± 0.007	22.19 ± 0.65	68.11 ± 1.25	17.11 ± 0.50	3.24
	Rev	1.137 ± 0.007	22.17 ± 0.66	70.17 ± 1.93	17.69 ± 0.41	
	Best	**1.135**	**22.69**	**71.59**	**18.43**	
MG (15 mg/mL)	Fwd	1.098 ± 0.005	21.60 ± 1.29	55.12 ± 1.44	13.08 ± 0.78	4.61
	Rev	1.109 ± 0.005	21.58 ± 1.27	57.36 ± 3.26	13.71 ± 0.78	
	Best	**1.107**	**22.91**	**57.89**	**14.68**	
MG (20 mg/mL)	Fwd	1.098 ± 0.011	20.74 ± 0.78	58.61 ± 2.29	13.34 ± 0.60	1.19
	Rev	1.104 ± 0.012	20.77 ± 0.83	58.89 ± 2.89	13.50 ± 0.68	
	Best	**1.104**	**21.63**	**59.26**	**14.15**	
MG-COOH (10 mg/mL)	Fwd	1.118 ± 0.007	22.13 ± 0.40	60.92 ± 3.63	15.07 ± 0.91	8.17
	Rev	1.126 ± 0.006	21.97 ± 0.43	66.35 ± 1.97	16.41 ± 0.59	
	Best	**1.129**	**22.91**	**68.55**	**17.73**	
UVO-MG (10 mg/mL)	Fwd	1.106 ± 0.010	22.72 ± 0.80	67.72 ± 2.51	17.01 ± 0.84	11.34
	Rev	1.119 ± 0.008	22.72 ± 0.80	75.53 ± 1.17	19.19 ±0.59	
	Best	**1.120**	**23.53**	**76.23**	**20.09**	

[a] $HI = [(PCE_{Rev} - PCE_{Fwd}) / PCE_{Rev}] \times 100$

Table S2. Parameters from fitting the time-resolved PL data[a]

Particle Concentration (%)	τ_{fast} **(ns)**	τ_{slow} **(ns)**	A **(Counts)**	B **(Counts)**	τ_{eff} **(ns)**
Control	13.91	97.95	100.58	319.57	77.83
MG (10 mg/mL)	-	195.6	-	216.47	195.6
MG (20 mg/mL)	-	219.4	-	233.74	219.4
MG-COOH (10 mg/mL)	-	199.4	-	230.1	199.4
UVO-MG (10 mg/mL)	13.89	137.24	99.13	313.84	107.63

[a] The parameters in the columns two to five are from Equation (2). The parameter in the last column is from Equation (3).

Table S3. Parameters from fitting the EIS data[a]

Particle Concentration (%)	R_s **(Ω)**	R_p **(Ω)**	C_p **(F)**
Control	11.4	393	3.32×10^{-9}
MG (10 mg/mL)	13.8	752	3.02×10^{-9}
MG (20 mg/mL)	14.8	1151	2.49×10^{-9}
UVO-MG (10 mg/mL)	12.9	427	3.50×10^{-9}

[a] The parameters were obtained by fitting the EIS data to the model shown in Fig. 3E.

Table S4. Students t-test analysis for the PCE data for systems studied.

Test	PCE data	**DF**[a]	***t***	***P* (0.001)**[b]	**Null hypothesis**
1	Control and UVO-MG-based devices	50	4.80	1.6×10^{-5}	Failed
2	MG- and UVO-MG-based devices	40	9.65	1.1×10^{-11}	Failed

[a] Degree of freedom. [b] The $t_{0.9995}$ threshold is 0.001 for upholding the null hypothesis.

References

1. A. Delplanque, E. Henry, J. Lautru, H. Leh, M. Buckle and C. Nogues, *Appl. Surf. Sci.*, 2014, **314**, 280-285.
2. L. Macmanus, M. Walzak and N. McIntyre, *J. Polym. Sci., Part A-1: Polym. Chem.*, 1999, **37**, 2489-2501.
3. T. N. Murakami, Y. Fukushima, Y. Hirano, Y. Tokuoka, M. Takahashi and N. Kawashima, *Appl. Surface Sci.*, 2005, **249**, 425-432.
4. A. Ross and V. L. Willson, *Basic and advanced statistical tests: Writing results sections and creating tables and figures*, Springer, 2018.
5. M. F. Triola, *Elementary statistics using Excel*, Pearson, 2013.